

Chemical Degradation of Screen-Printed Thick Films on LTCC

Nils Junker^{*1, 2}, Thomas J. Rabbow¹, Michael Schneider¹,
Jochen Schilm¹, Alexander Michaelis^{1, 2}

¹Fraunhofer-Institut für Keramische Technologien
und Systeme IKTS, Winterbergstrasse 28, 01277 Dresden, Germany

²Institut für Werkstoffwissenschaft, Technische Universität
Dresden, Helmholtzstrasse 7, 01069 Dresden, Germany

received March 5, 2014; received in revised form May 19, 2014; accepted May 27, 2014

Abstract

The degradation behavior of screen-printed thick films on LTCC was investigated in sulfuric and nitric acid. The samples were examined with regard to their mass loss as well as by means of scanning electron microscopy. Additionally, the eluates were analyzed with voltammetric and spectroscopic methods. In any case, the degradation is dominated by the dissolution of an aluminosilicate phase. The degradation in sulfuric acid is generally lower than in nitric acid, caused by kinetic inhibition owing to the formation of sulfates. Delamination of the thick film, resulting from the low chemical resistance of the interphase, occurred in the case of the composite-containing additives. No thick film delamination was observed on the additive-free composite. However, selective dissolution of the substrate's aluminosilicate phase takes place beneath the thick film.

Keywords: LTCC, thick film, degradation, chemical durability

I. Introduction

Screen-printed thick films (SPTF) on low-temperature co-firing ceramics (LTCC) are widespread in the manufacture of high-end microelectronics¹. SPTF are also commonly used as surface metallization on photovoltaic cells². Moreover, selective electrochemical sensors for different analytes (e.g. CO, O₂, H₂, H⁺) in gaseous and liquid media can be achieved with such SPTF^{3–5}. In recent years, several lab-on-a-chip devices for biomedical and environmental sensor applications have been developed using LTCC technology^{6–8}. LTCC technology also offers the possibility to design the 3D structures of microfluidic systems^{9, 10}. Furthermore, screen-printing technology allows additional functionalization of LTCC with the implementation of e.g. heaters or electrodes for sensor applications including complete electrochemical cells^{11–15}. The lifetime and reliability of such micro-technologic devices are strictly related to degradation processes. The thick films have to resist the (electro-)chemically induced strains, particularly in electrochemical environments or applications (e.g. galvanic reinforcement of screen-printed bus bars on solar cells)^{16, 17}. Localized degradation of only one of the screen-printed LTCC parts already can cause the failure of the whole device.

In literature LTCC is described as a chemically inert material^{8, 18, 19}. Although, the chemical resistivity of the glass components of screen-printing pastes has been investigated²⁰. However, there is still a lack of information about the chemical durability of the complete thick-film-LTCC

composite. The present study focuses on the impact of SPTF on the degradation behavior of these composites. Two model systems (with and without inorganic additives) were investigated. The results are compared with the degradation behavior of pure LTCC.

II. Experimental

In all experiments, DuPont 951 GTTM was used as a LTCC substrate material. The substrate was produced by the lamination of three single tapes. The stack has a dimension of 10 x 10 cm² and a thickness of 0.65 mm. The screen-printing process of the gold paste onto the substrate followed by a firing process (Table 1) completed the LTCC (screen printer: KEKO P200A, Slovenia; mesh count: 235; tube furnace: ATV PEO 603, Germany). The print layout is shown schematically in Fig. 1a. Two different gold pastes were used (DuPont 5742TM conductor paste and an in-house-produced paste). The DP5742TM paste contains glass components and several metal oxides^{16, 17} and was directly screen-printed onto the green substrate. A co-firing process at 875 °C was carried out for 60 min²¹. The in-house-produced gold paste was free of oxidic sintering additives, but it contained a very small amount of silver^{16, 17}. This paste was screen-printed and post-fired on an already sintered DP951GTTM substrate. All firing runs were carried out with the same firing regime that was used for the co-firing process. The finalized samples were dissected to a dimension of 30 x 8 mm² (total surface area = 5.3 cm²). The samples were exposed to 1 N H₂SO₄ and 1 N HNO₃ at 30 °C over a maximum of five days. The samples were exposed in PTFE vessels filled with a continuously stirred

* Corresponding author: nils.junker@ikts.fraunhofer.de

Table 1: Preparation parameters.

System	Material combination	Firing procedure		Thick-film-covered surface area A_{tf}	
		1 st run	2 nd run	absolute /cm ²	relative /%
A	DP951GT (blank)	LTCC	-	0	0
B	DP951GT + DP5742	LTCC + paste	-	0.30	5.7
C	DP951GT + in-house paste	LTCC	LTCC (fired) + paste	0.39	7.4

bath volume of 125 ml (Fig. 1). The specimens were fixed in a PTFE holder. Before and after the exposure, all samples were weighed with a Cubis MSE225S precision balance (Sartorius AG, Germany), which provides an accuracy of ± 0.015 mg. After the exposure experiment, the concentration of leached metal ions in the eluates was determined by means of voltammetric measurements with a VA Computrace 797 polarograph (Metrohm, Switzerland). A differential pulse adsorptive sweep voltammetry (DPAdSV) was performed for the determination of Al^{3+} . Cu^{2+} , Pb^{2+} and Bi^{3+} were determined with differential pulse anodic sweep voltammetry (DPASV). Each eluate solution was measured three times. The standard deviation was $\leq 5\%$. Additionally, selected samples were investigated for Al^{3+} , Si^{4+} and Ca^{2+} by ICP-OES (ERGO Umweltinstitut Dresden, Germany), and with a field emission scanning electron microscope (FESEM) Ultra 55 (Carl Zeiss, Germany), respectively. The EDX analysis was performed with a Si(Li)-detector (Oxford Instruments, UK). Quantitative X-ray fluorescence analysis (XRF) was only performed on the unexposed and blank substrate material, using a S8 TIGER spectrometer (Bruker, USA).

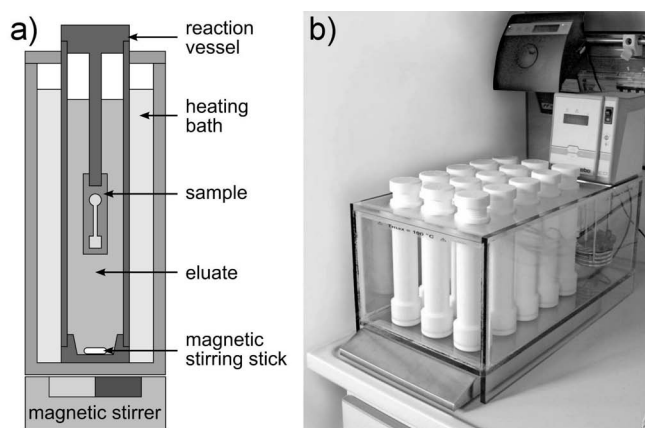


Fig. 1: Exposure apparatus: a) schematic drawing of a single unit, b) multiple array.

III. Results and Discussion

(1) Visual evaluation

Degradation was observed in all systems, which is noticeable from the bleaching of the LTCC (Fig. 2; System A is not shown). The blue-greenish surface color brightened over the exposure time (visible as a gradual brightening of the dark gray surface in Fig. 2). The degradation was inhibited in the area covered by the sample holder. The intensity

of the bleaching was slightly stronger in nitric acid than in sulfuric acid.

The degradation of System B could also be recognized by the delamination of the thick film. Partial delamination of the thick film in sulfuric acid appeared after four days. After five days the thick film was completely delaminated. In nitric acid, the complete delamination of the thick film had already occurred after two days. Additionally, the substrate area beneath the delaminated thick film was more strongly bleached than the uncovered area. System C showed no delamination, in contrast to System B.

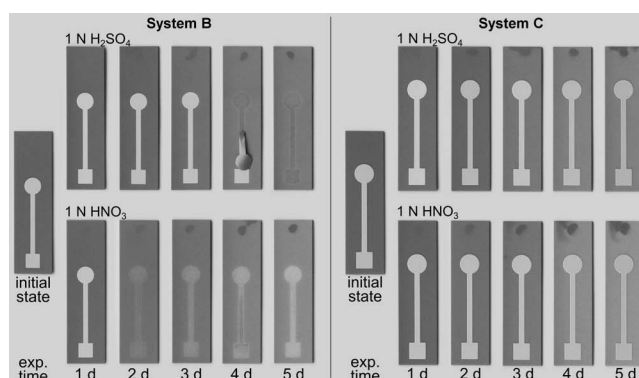


Fig. 2: Systems B and C before and after exposure.

(2) Quantitative analyses

A quantitative screening of the mass loss and the leached metal ions is necessary to achieve more detailed information on the degradation process. Table 2 shows the chemical composition of the substrate, determined by means of XRF analysis. The result was compared with the EDX analysis of such material as reported by Chan *et al.*²². All substrates consist mainly of an aluminosilicate glass phase, filled with alumina particles (the microstructure is discussed more in detail in Section III(3)). Owing to the fact that the substrate represents $\approx 93 - 94\%$ of the composite's total surface area, the degradation behavior of the blank substrate will be discussed first.

Fig. 3 shows the mass loss of System A. In both acids, the mass loss increases with ongoing exposure time. However, the mass loss is lower in sulfuric acid than in nitric acid. This behavior agrees with the visual evaluation of the samples. In sulfuric acid the blank substrate shows a mass loss of 55 and 265 μgcm^{-2} over the exposure times of one day and five days, respectively. These are approximately three quarters of the mass loss observed in nitric acid. This difference can be explained by the formation of sparsely soluble $PbSO_4$ and $CaSO_4$ in sulfuric acid (Table 3). According

to Seidel *et al.*²³, it can be assumed that PbSO₄ and CaSO₄ are formed as a metastable barrier layer during the exposure in sulfuric acid, which leads to an inhibition. In nitric acid, in turn, Pb(NO₃)₂ and Ca(NO₃)₂ are formed which are easily soluble (Table 3) and do not form a barrier layer.

Table 2: Chemical composition of the LTCC substrate (in wt%).

Oxide	XRF		EDX (Lit. 22)
	Amount	Error	
Al ₂ O ₃	50.70	±0.111	50.3
SiO ₂	31.60	±0.085	31.3
PbO	10.28	±0.006	11.9
CaO	4.23	±0.015	5.4
Na ₂ O	1.46	±0.035	-
K ₂ O	1.02	±0.008	1.1
CoO	0.27	±0.001	-
Cr ₂ O ₃	0.26	±0.003	-

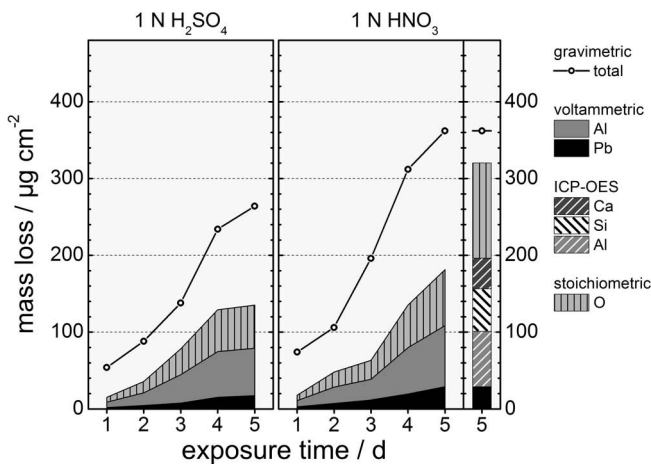


Fig. 3: Total mass loss and enrichment of metal ions of System A in 1 N H₂SO₄ and 1 N HNO₃ over exposure time.

Table 3: Solubility of the sulfates and the nitrates from lead and calcium.

Sulfate	sol. in 1 N H ₂ SO ₄		Lit.	sol. in H ₂ O		Lit.
		T /°C			T /°C	
PbSO ₄	6–10 mg l ⁻¹	30	24	47 mg l ⁻¹	30	25
CaSO ₄	3.1 gl ⁻¹	25	26	2.1 gl ⁻¹	30	25
Nitrate	sol. in 1 N HNO ₃		Lit.	sol. in H ₂ O		Lit.
		T /°C			T /°C	
Pb(NO ₃) ₂	285 gl ⁻¹	25	27	457 gl ⁻¹	25	27
Ca(NO ₃) ₂	-	-	-	990 gl ⁻¹	30	25, 28

As shown in Fig. 3, Al³⁺ and Pb²⁺ are enriched in the solution with ongoing exposure, following the curve pro-

gression of the total mass loss. The concentration of Al³⁺ is similar in both sulfuric and nitric acid. After five days, the concentration of Pb²⁺ is half as high in sulfuric acid as in nitric acid owing to the formation of metastable PbSO₄. Assuming that the degradation is characterized by hydrolysis, the cumulative share of Al³⁺, Pb²⁺ and O²⁻ amounts to ≈ 30 % and ≈ 52 % of the total mass loss after one day and after five days, respectively, in sulfuric acid. In nitric acid, it constitutes ≈ 25 % and ≈ 50 %, respectively. The part of Al³⁺ and Pb²⁺, with reference to the total mass loss, increases in both acids with ongoing exposure. This behavior is probably associated with a change of the degradation mechanism. In the early stage, interdiffusion processes of the framework changers of the glass phase – Na⁺, K⁺, and Ca²⁺ – mainly characterize the degradation. After about two days, the destruction of the framework becomes the dominating process. The ICP-OES measurements fill the mismatch to the total mass loss in nitric acid. After five days, 56 µgcm⁻² of Si⁴⁺ and 38 µgcm⁻² of Ca²⁺ are leached out from the substrate. The value of 70 µgcm⁻² Al³⁺ (ICP-OES) is in a good agreement with the value of 74 µgcm⁻² detected by means of voltammetry. The amounts of Al³⁺, Si⁴⁺, Pb²⁺, Ca²⁺ and O²⁻ in total cover approximately 89 % of the total mass loss. The remaining gap can be explained by the non-determined shares of Na₂O and K₂O (2.5 wt% of the LTCC material; Table 2).

Fig. 4 shows the degradation behavior of System B. In sulfuric acid, the mass loss as well as the eluate concentration of Al³⁺ and Pb²⁺ are comparable with System A. Again, in nitric acid, System B shows higher degradation rates than System A. Furthermore, the difference between Systems A and B, concerning the concentration of Al³⁺, increases with ongoing exposure time. However, the difference concerning the concentration of Pb²⁺ decreases. Additionally, the concentrations of Si⁴⁺, Ca²⁺ and Al³⁺ determined with ICP-OES are about 13 %, 21 % and 14% higher in comparison with System A. The difference between the spectroscopically and voltammetrically determined Al³⁺ contents amounts to approximately 27 %. With respect to the different limits of quantitation for Al³⁺ (DPAdSV²⁹: 3 µgl⁻¹; ICP-OES³⁰: 0.1 mg l⁻¹), it can be assumed that the concentration of Al³⁺ is underdetermined with ICP-OES.

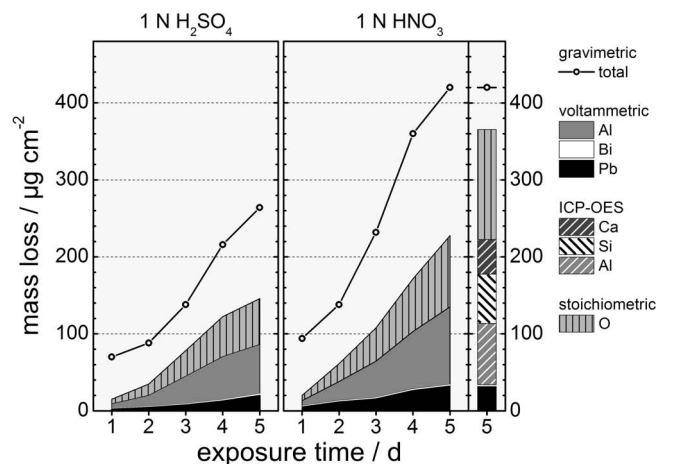
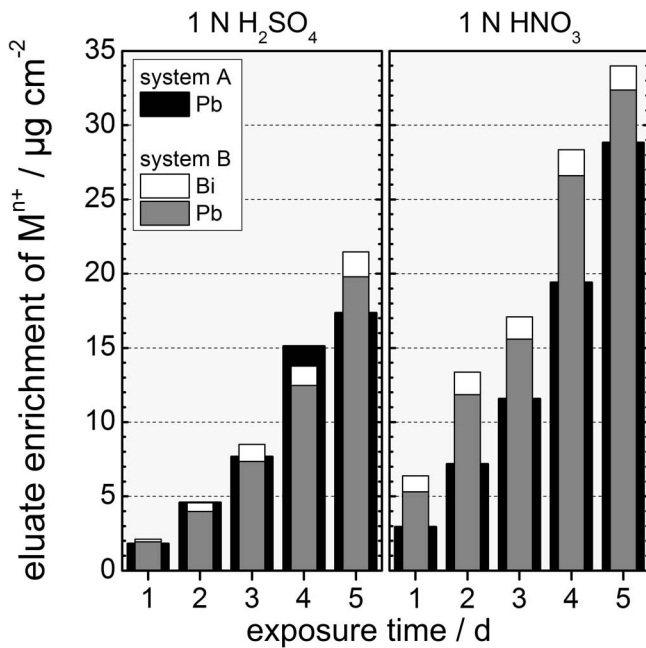


Fig. 4: Total mass loss and enrichment of metal ions of System B in 1 N H₂SO₄ and 1 N HNO₃ over exposure time.

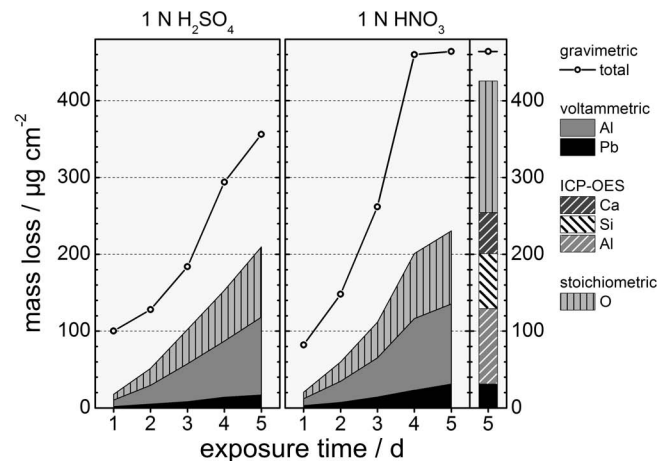
Table 4: Eluate containing $\text{Al}^{3+}/\text{Pb}^{2+}$ ratio after exposure times of one and five days.

System	Material combination	Firing runs	$\text{Al}^{3+}/\text{Pb}^{2+}$ ratio (mass-related)			
			1 N H_2SO_4		1 N HNO_3	
			1 day	5 days	1 day	5 days
A	DP951GT (blank)	1	3.9	3.6	2.6	2.8
B	DP951GT + DP5742	1	3.6	3.3	1.3	3.1
C	DP951GT + in-house paste	2	4.2	6.0	3.0	3.3

The DP5742 gold paste contains oxides of Bi and Cu as sintering additives^{16,17}. It is reasonable to suggest that these oxides are part of the interphase between the substrate and the thick film. As Fig. 5 shows, the content of Bi^{3+} increases in both acids with ongoing exposure, but a steady state obviously exists when a level of about $1.7 \mu\text{gcm}^{-2}$ is reached. If we assume that bismuth exclusively originates from the thick film (see also Table 2), the value of $1.7 \mu\text{gcm}^{-2}$ roughly corresponds to a content of $30 \mu\text{gcm}^{-2}$ Bi in the thick film. If Bi^{3+} exceeds a critical leaching amount of about $1.4 \mu\text{gcm}^{-2}$ ($\approx 25 \mu\text{gcm}^{-2}$ thick film area), delamination appears. This fact is independent of the acid (see also Fig. 2). Traces of Cu^{2+} could not be quantitatively determined in both eluates. Comparably to System A, the amounts of Al^{3+} , Si^{4+} , Ca^{2+} , Pb^{2+} , Bi^{3+} and O^{2-} result in $\approx 91\%$ of the total mass loss. This means that the degradation mainly takes place at the substrate. Nevertheless, the stronger degradation of System B in nitric acid might be caused by a lower chemical durability of the interphase LTCC substrate/thick film.

**Fig. 5:** Voltammetrically determined eluate concentrations of Pb^{2+} and Bi^{3+} of Systems A and B.

The mass loss of System C also increases in both acids with ongoing exposure (Fig. 6). Although the course is comparable to both Systems A and B, the absolute values are significantly higher.

**Fig. 6:** Total mass loss and enrichment of metal ions of System C in 1 N H_2SO_4 and 1 N HNO_3 over exposure time.

In sulfuric acid, the mass loss of System C is stronger than that of System B. If the mass loss of System B is set to 100 %, the mass losses of System C amount to $\approx 150\%$ and $\approx 131\%$ after one and five days, respectively.

Indeed, the mass losses of System C are $\approx 85\%$ and $\approx 35\%$ higher than those of System A (normalized to be 100 %). Surprisingly, the leached amount of Pb^{2+} is almost equal among all systems, and it varies in a range of ± 0.1 and $\pm 1.5 \mu\text{gcm}^{-2}$. This behavior is completely different to the leaching of Al^{3+} . Initially, the amount of dissolved Al^{3+} deviates in the range of $\pm 0.7 \mu\text{gcm}^{-2}$ among all systems. After five days of exposure the amount of Al^{3+} leached from System C is $\approx 57\%$ and $\approx 65\%$ higher than in case of Systems B and A. In nitric acid those differences are less pronounced than in sulfuric acid. The mass loss is $\approx 10\%$ and $\approx 27\%$ higher in comparison with Systems B and A after five days of exposure. Briefly speaking, System C shows the highest amounts of dissolved Al^{3+} . Simultaneously, the amounts of Pb^{2+} leached out of System C are lower than in the case of System B. This behavior takes place as a result of the dissolution of the Pb-containing interphase of System B. Additional information is given by comparing the $\text{Al}^{3+}/\text{Pb}^{2+}$ ratio of the eluates (Table 4): A strong Al^{3+} leaching is obviously connected to the re-firing process, the lower Pb^{2+} content in sulfuric acid is a consequence of the metastable PbSO_4 -formation.

The shares of Al^{3+} , Si^{4+} , Ca^{2+} , Pb^{2+} and O^{2-} amount to 92 % of the total mass loss. This corresponds to the other materials. System C shows the highest mass loss and cumulative leaching amounts in both acids. Nevertheless, the

thick film does not delaminate during exposure (Fig. 2). This property is obviously restricted to the use of a glass-free paste, and will be discussed in detail in Section III(3).

(3) Microstructure

The microstructure of the LTCC substrate material (Fig. 7) consists of five phases. Homogeneously distributed corundum particles with a diameter of 1–5 μm (1) make up the major phase. These particles are embedded in an amorphous aluminosilicate matrix (2). A second aluminosilicate phase, which is enriched in Al, is formed around the corundum particles during the sintering process (3). This phase forms a 3D network which pervades the complete material. Accompanying this, homogeneously distributed $\text{Co}(\text{Al,Cr})_2\text{O}_4$ particles with a diameter of 0.1–0.5 μm exist (4). These particles are responsible for the blue-greenish color of the substrate. Furthermore, pores (5) and small, scattered particles of SiO_2 (presumably cristobalite) are detectable (6).

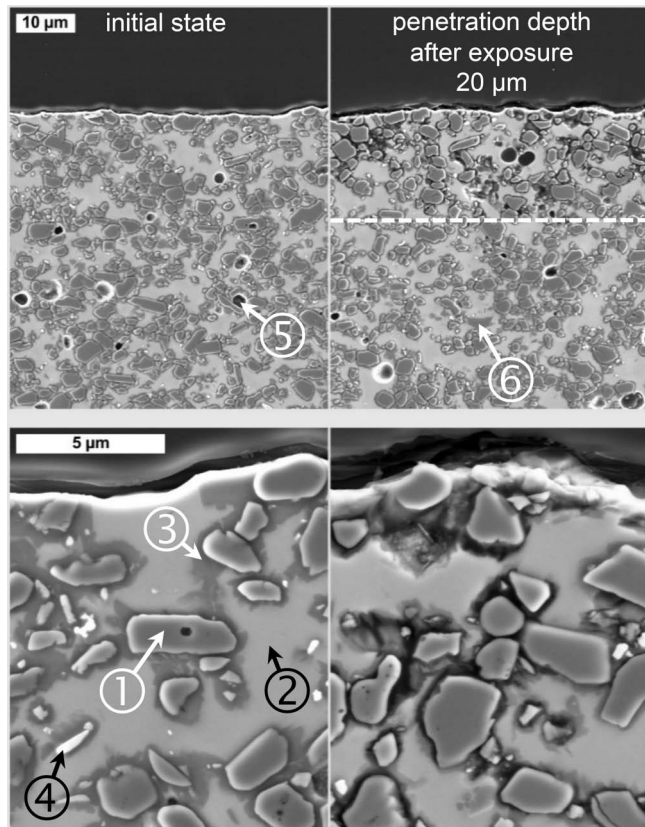


Fig. 7: Scanning electron micrographs of System A before and after an exposure time of five days in 1 N HNO_3 (top: overview; bottom: detailed view).

The phase around the corundum particles is selectively dissolved under acidic conditions. This is in good agreement with Bittner *et al.*³¹ who specified this phase as anorthite ($\text{CaAl}_2\text{Si}_2\text{O}_8$). Also Hrovat *et al.*¹² determined anorthite in DP951GTTM, but with a small amount of sodium ($(\text{Na,Ca})(\text{Al,Si})_4\text{O}_8$). Assessing the reported XRD spectra^{12,31}, the reflexes referred to are similar within the whole plagioclase feldspar supergroup^{32,33}. In the present work the EDX spectra (Fig. 8) suggest that the dissolved phase (No.3 in Fig. 7) consists of a

combination of plagioclase feldspars with traces of Pb. The stoichiometric composition of this phase is hypothesized to be $\text{Na}_{0.2}\text{Ca}_{0.3}\text{Pb}_{0.05}\text{Al}_{2.8}\text{Si}_{1.7}\text{O}_{8.1}$, based on the EDX analysis (Fig. 8). Based on the kinetic data shown in Fig. 3, the leaching process becomes diffusion-controlled with increasing penetration depth. According to the literature^{31,34}, the dissolution occurs by hydrolysis:

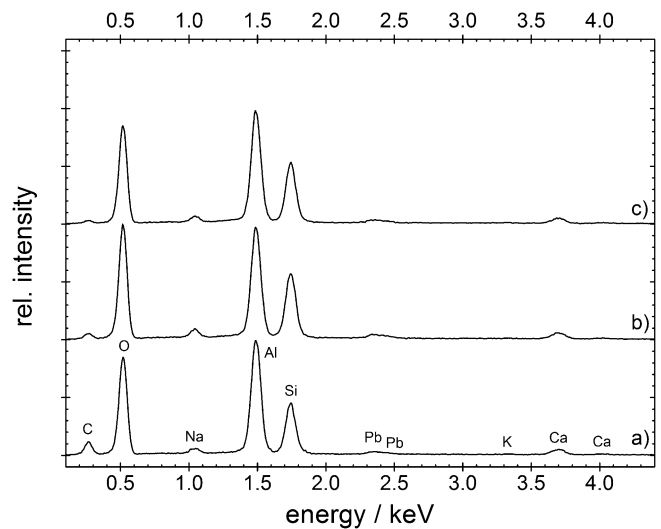
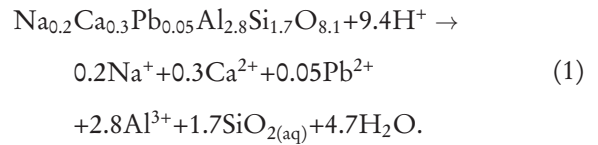


Fig. 8: EDX spectra obtained with spot measurements at the aluminum-rich phase of Systems A (a), B (b) and C (c).

This phase shows a stoichiometric ratio of 1.65 between Al and Si. In contrast, anorthite and albite show a ratio Al/Si of 1/1 and 1/3, respectively. Oelkers *et al.* found that the hydrolysis resistance of plagioclase feldspars decreases with an increasing Al/Si ratio³⁴. The lower chemical resistance is caused by a higher number of weak Al-O-bridges within the Si-O-Al-O-framework. The stoichiometry of the non-dissolved, aluminum-poor aluminosilicate (No.2 in Fig. 7) is approximately $\text{Na}_{0.08}\text{K}_{0.16}\text{Ca}_{0.15}\text{Pb}_{0.26}\text{Al}_{0.6}\text{Si}_{3.3}\text{O}_{8.03}$, considering the EDX spectra a) and c) in Fig. 9. The Al/Si ratio is only 0.18, which explains the strong hydrolysis resistance of this phase. Furthermore, it cannot be excluded that Pb^{2+} is dissolved from the interface aluminum-poor/aluminum-rich aluminosilicate.

Although the surface of the substrate was bleached out with ongoing exposure, $\text{Co}(\text{Al,Cr})_2\text{O}_4$ particles are still present, as the micrographs of the cross-section show. Therefore the aluminum-rich aluminosilicate has a strong impact on the optical properties of the material. Owing to the dissolution process, the interface area of the incorporated $\text{Co}(\text{Al,Cr})_2\text{O}_4$ pigments is decreased, which leads to the observed bleaching effect.

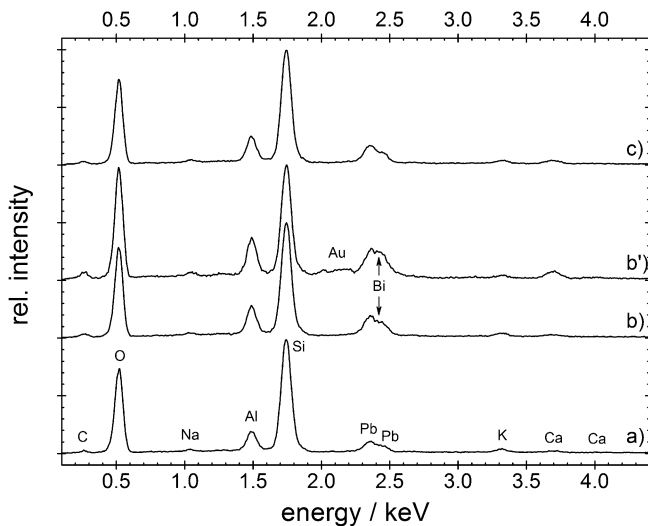


Fig. 9: EDX spectra obtained with spot measurements at the aluminum-poor phase of Systems A (a), B (b = 6 μm and b' = 1 μm below the thick film) and C (c).

The microstructure of System B (Fig. 10) is more complex than that of the blank substrate. The thick film consists of a gold matrix with incorporated metal oxides and silicates^{16,17}. Moreover, an interphase is formed between the thick film and the substrate during the firing process. The thickness of the interphase measures approximately 5–10 μm and is smoothly merged into the substrate's aluminosilicate matrix, which is indicated by a certain Bi content. (The gap between the thick film and the interphase visible in Fig. 10 is caused by the grinding preparation.)

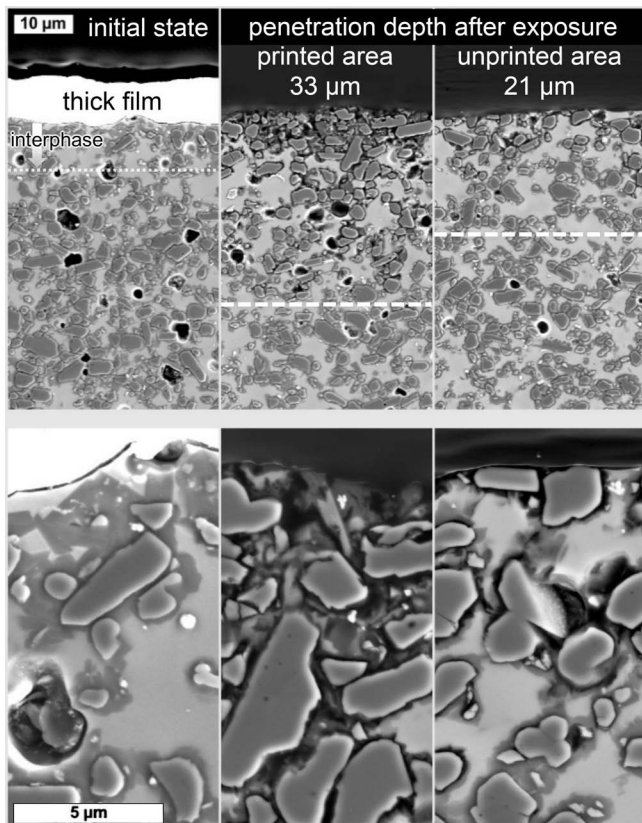
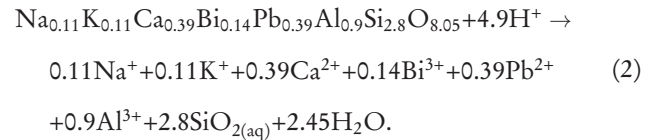


Fig. 10: Scanning electron micrographs of System B before and after an exposure time of five days in 1 N HNO_3 (top: overview; bottom: detailed view).

The degradation behavior of the unprinted area of System B (Fig. 10, right) is comparable to that of the blank substrate (Fig. 7, right). A strong degradation, associated with penetration as deep as 33 μm , can be observed at the interphase (Fig. 10, center). The delamination of the thick film is caused by the dissolution of this Bi^{3+} -containing interphase. According to Eq. 1 and in respect of the EDX spectrum b) in Fig. 9, the following hydrolysis reaction can be assumed:



The film adhesion of System C is directly enabled by the aluminosilicate phases of the substrate (Fig. 11, left). Only the aluminum-rich aluminosilicate is selectively dissolved from the substrate. A penetration depth of 25 μm is observed (Fig. 11, right) on the unprinted area. This is $\approx 20\%$ deeper than observed in the case of the other systems. However, beneath the thick film the material has been undermined by the acid and severely destroyed down to a depth of 16 μm (Fig. 11, center). This also explains the easy delamination of the thick film during the preparation of the sample for FESEM. However, neither an expansion nor a more pronounced framework of the aluminum-rich aluminosilicate phase after the post-firing process is observed. Therefore, it can be assumed that this phase was restructured within the second firing run, resulting in a hydrolysis resistance that is weaker than in the case of co-fired substrates.

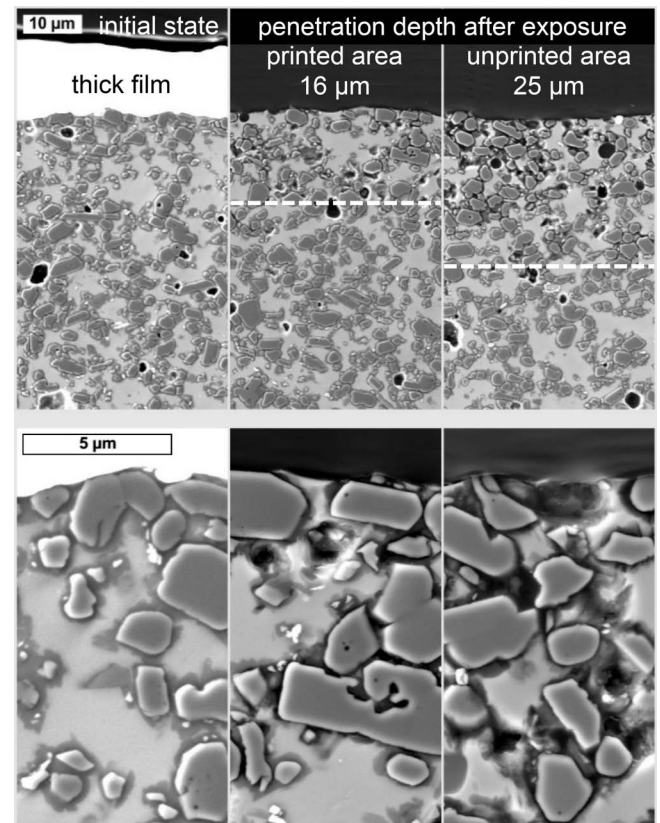


Fig. 11: Scanning electron micrographs of System C before and after an exposure time of five days in 1 N HNO_3 (top: overview; bottom: detailed view).

IV. Conclusions

The degradation process of screen-printed thick films on LTCC in acids is primarily characterized by the selective dissolution of an aluminum-rich aluminosilicate phase of the substrate. With ongoing exposure, the degradation process becomes more and more diffusion-controlled, owing to the dissolution of the 3D network of the aluminum-rich aluminosilicate. Generally, the degradation of the material in sulfuric acid is inhibited as sparsely soluble sulfates are formed. Post-fired LTCC dissolves more strongly. This behavior is probably caused by a phase reconfiguration during the re-firing process. Nevertheless, the delamination is only occurred in the system with the glass-containing thick film. It is shown that the chemical durability of the interphase of this composite is lowered by the Bi₂O₃-containing gold paste. Thus the application of SPTF on LTCC (DP951GT™ substrate) for sensors as well as in plating processes is restricted to pH-neutral media, considering that even the substrate shows merely low chemical resistance in diluted acids. With respect to electrochemical applications, e.g. plating, a decrease of the pH value caused by electrode reactions (e.g. oxygen evolution) in front of the electrode must be avoided.

Acknowledgement

The financial support by the German Research Foundation (DFG) in the scope of the project “Electrochemical behavior and degradation of screen-printed metal-ceramic material composites” (MI509/11 – 1, SCHN745/8 – 1) is gratefully acknowledged.

References

- 1 Imanaka, Y.: Multilayered low temperature cofired ceramics (LTCC) Technology, Springer, Boston, MA, 2005.
- 2 Schubert, G., Huster, F., Fath, P.: Physical understanding of printed thick-film front contacts of crystalline si solar cells – review of existing models and recent developments, *Sol. En. Mat. Sol. C.*, **90**, 3399–3406, (2006).
- 3 Prudenziati, M.: Thick-film technology, *Sens. Act. A: Phys.*, **25**, 227–234, (1990).
- 4 Gac, A., Atkinson, J.K., Zhang, Z., Sion, R.P.: A comparison of thick-film chemical sensor characteristics in laboratory and on-line industrial process applications, *Meas. Sci. Techn.*, **13**, 2062–2073, (2002).
- 5 Malyshev, V.V., Pislyakov, A.V.: Dynamic properties and sensitivity of semiconductor metal-oxide thick-film sensors to various gases in air gaseous medium, *Sens. Act. B: Chemical*, **96**, 413–434, (2003).
- 6 Fakunle, E., Fritsch, I.: Low-temperature co-fired ceramic microchannels with individually addressable screen-printed gold electrodes on four walls for self-contained electrochemical immunoassays, *Anal. Bioanal. Chem.*, **6**, 2605–2615, (2010).
- 7 Gongora-Rubio, M.R., Fontes, M.B.A., da Rocha, Z.M., Richter, E.M., Angnes, L.: LTCC manifold for heavy metal detection system in biomedical and environmental fluids, *Sens. Act. B: Chem.*, **103**, 468–473, (2004).
- 8 Vasudev, A., Kaushik, A., Jones, K., Bhansali, S.: Prospects of low temperature co-fired ceramic (LTCC) based microfluidic systems for point-of-care biosensing and environmental sensing, *Microfluid. Nanofluid.*, **14**, 683–702, (2013).
- 9 Gross, G.A., Thelemann, T., Schneider, S., Boskovic, D., Köhler, J.M.: Fabrication and fluidic characterization of static micromixers made of low temperature cofired ceramic (LTCC), *Chem. Engin. Sci.*, **63**, 2773–2784, (2008).
- 10 Czok, M.J., Tadaszak, R.J., Bembnowicz, P.I., Golonka, L.J.: LTCC based chip for monitoring in biological applications, *Sens. Act. B: Chem.*, **189**, 118–122, (2013).
- 11 Nowak, D., Dziedzic, A.: LTCC package for high temperature applications, *Microelec. Rel.*, **51**, 1241–1244, (2011).
- 12 Hrovat, M., Belavič, D., Kita, J., Cilensšek, J., Golonka, L., Dziedzic, A.: Thick-film temperature sensors on alumina and LTCC substrates, *J. Eur. Ceram. Soc.*, **25**, 3443–3450, (2005).
- 13 Malecha, K., Pijanowska, D.G., Golonka, L.J., Torbicz, W.: LTCC microreactor for urea determination in biological fluids, *Sens. Act. B: Chem.*, **141**, 301–308, (2009).
- 14 Goldbach, M., Axthelm, H., Keusgen, M.: LTCC-based microchips for the electrochemical detection of phenolic compounds, *Sens. Act. B: Chem.*, **120**, 346–351, (2006).
- 15 Pesquero, N.C., Gongora-Rubio, M.R., Yamanaka, H.: A novel LTCC electrochemical cell construction and characterization: a detection compartment for portable devices, *Analyst*, **138**, 4298–4304, (2013).
- 16 Rabbow, T., Junker, N., Kretzschmar, C., Schneider, M., Michaelis, A.: Electrochemically induced degradation of screen-printed gold thick films, *J. Ceram. Sci. Techn.*, **3**, 199–210, (2012).
- 17 Rabbow, T.J., Junker, N., Schneider, M., Michaelis, A.: Screen-printed gold thick films for electrochemical sensor applications, *Mat. Sci. Engin. Techn.*, **42**, 777–783, (2011).
- 18 Gongora-Rubio, M.R., Espinoza-Vallejos, P., Sola-Laguna, L., Santiago-Avilés, J.J.: Overview of low temperature co-fired ceramics tape technology for meso-system technology (MsST), *Sens. Act. A: Phys.*, **89**, 222–241, (2001).
- 19 Malecha, K., Gancarz, I., Golonka, L.J.: A PDMS/LTCC bonding technique for microfluidic application, *J. Micromech. Microeng.*, **19**, 105016, (2009).
- 20 Mattox, D.M., Robinson, J.H.: Chemical durability of lead-oxide-based, thick-film binder glasses, *J. Am. Ceram. Soc.*, **80**, 1189–1192, (1997).
- 21 DuPont Microcircuit Materials: DuPont 951 Green Tape™ data sheet, 2001, http://www2.dupont.com/MCM/en_US/assets/downloads/prodinfo/951LTCCGreenTape.pdf, (accessed 18 November 2013).
- 22 Chan, Y.C., Li, C.Y.: Fabrication and characterization of multilayer capacitors buried in a low temperature co-fired ceramic substrate, *Act. Pass. Elec. Comp.*, **20**, 215–224, (1998).
- 23 Seidel, A., Slusznay, A., Shelef, G., Zimmels, Y.: Self inhibition of aluminum leaching from coal fly ash by sulfuric acid, *Chem. Engin. J.*, **72**, 195–207, (1999).
- 24 Pavlov, D., Pashmakova, I.: Influence of the size of PbSO₄ crystals on their solubility and the significance of this process in the lead-acid battery, *J. Appl. Electrochem.*, **17**, 1075–1082, (1987).
- 25 Haynes, W.M.: CRC handbook of chemistry and physics: A ready-reference book of chemical and physical data, 94th edition. CRC Press, Boca Raton, 2013.
- 26 Azimi, G., Papangelakis, V.G., Dutrizac, J.E.: Modelling of calcium sulphate solubility in concentrated multi-component sulphate solutions, *3rd Fluid Properties Challenge*, **260**, 300–315, (2007).
- 27 Ostanova, S.V., Drozdov, S.V., Pashkov, G.L., Kholmogorov, A.G., Patrushev, V.V., Chumakov, V.G., Chubarov, A.V.: Solubility of lead nitrate in aqueous solutions of nitric acid and Iron(III) nitrate, *Russ. J. App. Chem.*, **74**, 1753–1755, (2001).
- 28 Green, D.W.: Perry’s chemical engineers’ handbook. 8th edition. McGraw-Hill, New York, 2008.
- 29 Metrohm: VA Application work AW CH4–0494–122009: Determination of Al in tap water by adsorptive stripping voltammetry, 2009.
- 30 Mills, I.: Plant analysis procedures. Kluwer Academic Publishers, Dordrecht, Boston, 2004.

- ³¹ Bittner, A., Schmid, U.: The porosification of fired LTCC substrates by applying a wet chemical etching procedure, *J. Eur. Ceram. Soc.*, **29**, 99–104, (2009).
- ³² ICDD: Powder diffraction file no. 00–009–0466, Albite, ordered, CuK α 1.5405 Å, (2010).
- ³³ ICDD: Powder diffraction file no. 00–041–1486, Anorthite, ordered, CuK α 1.5405 Å, (2010).
- ³⁴ Oelkers, E.H., Schott, J.: Experimental study of anorthite dissolution and the relative mechanism of feldspar hydrolysis, *Geochim. Cosmochim. Act.*, **59**, 5039–5053, (1995).